

Type I $F_A(R_b^+, C_s^+)$ and Type II $F_A(L_i^+, N_a^+)$ Tunable Laser activity and Interaction of Halogen Atoms (F, Cl, Br, I, At) at the (001) Surface of KBr Crystal: *ab Initio* Calculations

A.M. El-Mahdy *

Faculty of Education, Department of Physics, Ain Shams University,
Roxy, Cairo, Egypt

The effects of type I $F_A(R_b^+, C_s^+)$ and type II $F_A(L_i^+, N_a^+)$ color centers on tunable laser activity and adsorbate–substrate interactions of halogen atoms (F, Cl, Br, I, At) at the (0 0 1) surface of KBr, are investigated by using quantum mechanical CI singles and DFT *ab initio* methods. Clusters of variable sizes were embedded in the simulated Coulomb fields that closely approximate the Madelung fields of the host surface, and ions that were the nearest neighbors to the defect site were allowed to relax to equilibrium in order to calculate the optical properties. The sensitivity of the calculated transition energies (Stokes shifts) of Type I $F_A(R_b^+, C_s^+)$ and Type II $F_A(L_i^+, N_a^+)$ laser as well as related optical properties such as relaxed excited states orientational bleaching, defect formation energies, exciton (energy) transfer, and the Glasner–Tompkins empirical rule, to the coordination number of the surface ion were examined. The effects of F and F_A center on the halogen atom surface interaction as well as the relative roles of energy gaps and spin pairing in the course of adsorbate–substrate interactions were examined.

1. Introduction:

Fritz and Menke [1] showed that it was possible to observe a laser emission in a flash-lamp pumped rod containing F_A (II) centers i.e. F -centers associated with a small radius substitutional cationic impurity and characterized by an emission at a much larger wave-length than classical F -centers. In 1974, Mollenauer and Olson [2] pumped the same material with a krypton laser and started the field of continuous wave tunable color center lasers. In F_A centers [3] the three-fold degenerate 2p state of the F -center is split in absorption due to the adjacent cationic impurity, thus forming two well-resolved absorption transitions " F_{A1} band " and " F_{A2} band ". Two types of centers are therefore distinguished corresponding to the different relaxation behavior of the centers

after optical excitations: in type I F_A centers, F - centers are attached to a large-size cationic impurities, and in type II F centers, F - centers are attached to a small-size cationic impurities relative to the host cation.

For tunable laser applications, the electron-phonon coupling provides the most important property of broadened Stokes-Shifted optical transition bands between absorption and emission and an almost ideal four energy level scheme [4]. Consider the working principle of a dye laser which uses the optical pumping of F -centers yielding a four-level system. The optical pumping consists of four steps; excitation, relaxation of excited states, emission and relaxation to the ground state. The only populations of any significance are the populations of the relaxed ground state and excited states respectively. The question of whether efficient laser oscillation can be obtained with a specific center depends on non-interfering of the pumping cycle from a four energy level diagram [5].

The most important physical property of any material considered for tunable laser applications is the existence of strong and broad optical transitions. The electrons associated with a defect interact strongly with the surrounding vibrating crystal ions, resulting in optical transitions, which are allowed in a broad band around the defect specific central transitions. All color center lasers realized so far are based on electronic defects. Until recently the potential of F_A color centers for useful laser action had been ignored as far as first principal calculations are concerned. The first aim of this paper is, therefore, to examine the effects of the size of the impurity cation (adjacent to F_A center) on the laser activity at the KBr surface, in addition to some related properties such as RES orientational bleaching, defect formation energies, exciton (energy) transfer and Glasner–Tompkins relation and the relative positions of the RESs with respect to the conduction band of the perfect crystal using *ab initio* methods of molecular electronic structure calculations.

Understanding the nature of adsorbate–substrate interactions is of great importance in fields such as catalysis, corrosion, gas sensors and microelectronics. In general, adsorbate–substrate interactions result from the tendency of the adsorbate valence electrons to interact with the available substrate electrons. This interaction can be expected to have a major role if there exists a small energy gap between adsorbate and substrate surface, or if the adsorbate has an open shell electronic configuration where spin pairing occurs. However, very little is yet known about the adsorptivity of the halogen series F, Cl, Br, I and At on KBr surfaces. We have therefore performed a fairly extensive set of density functional theory (DFT) calculations. The second aim of this paper is, therefore, to shed light on the effects of F and F_A center on the

halogen atom surface interaction as well as the relative roles of energy gaps and spin pairing in the course of adsorbate–substrate interactions.

The present study is organized as follows: In Section 2 we present some aspects of the computational methods used to calculate the relevant properties. In Section 3 we discuss the results of our calculations. Finally, conclusions are presented in Section 4.

2. Methods:

2.1. Crystal Simulation:

There are several methods to simulate crystals, either by finite or infinite systems [6–11]. In the case of finite systems, only local portions of the crystal are considered. For such an approach, clusters of varying sizes in the bulk or surface structures are suitable approximations.

2.1.1. Bulk simulation.

To simulate the ionic crystal bulk, We follow a procedure previously reported for alkali halide and alkaline earth oxides [12–14]. A finite ionic crystal of 288 point charges was first constructed. The Coulomb potentials along the X and Y axes of this crystal are zero by symmetry as in the host crystal. The ± 1 charges on the outer shells listed in Table 1 were then modified, using a fitting procedure, to make the Coulomb potential at the four central sites closely approximate the Madelung potential of the host crystal, and to make the Coulomb potential at the eight points with coordinates $(0, \pm R, \pm R)$ and $(\pm R, 0, \pm R)$ where R is half the lattice distance, which for KBr is 3.298\AA , equal to zero as it should be in the host crystal. With charges, 0.409283 and 0.800909, the Coulomb potential in the region occupied by the central ions is very close to that in the unit cell of the host crystal. The Coulomb potential was calculated to be (1.748) at the four central sites (compared with 1.746 for an alkali halide ionic crystal) and (0.0) at the previously defined eight points (compared with 0.0 for the ionic crystal).

2.1.2. Surface simulation.

The low coordinated surfaces of the KBr crystal represented in Fig. (1) were then generated as follows:

1. All charged centers with Cartesian coordinates $(\pm X)$, $(\pm Y)$ and $(Z > 0)$ were eliminated to generate a flat surface with 176 charged centers occupying the three-dimensional space $(\pm X), (\pm Y)$ and $(Z \leq 0)$.

2. All charged centers with Cartesian coordinates $(\pm X)$, $(Y > 1)$ and $(Z > 0)$ were eliminated to generate an edge with 121 charged centers occupying the three-dimensional space $(\pm X)$, $(Y \leq 1)$ and $(Z \leq 0)$.
3. All charged centers with Cartesian coordinates $(-X < 1)$, $(Y > 1)$ and $(Z > 0)$ were eliminated to generate the Br^- corner with 81 charged centers occupying the three-dimensional space $(-X \geq 1)$, $(Y \leq 1)$ and $(Z \leq 0)$.

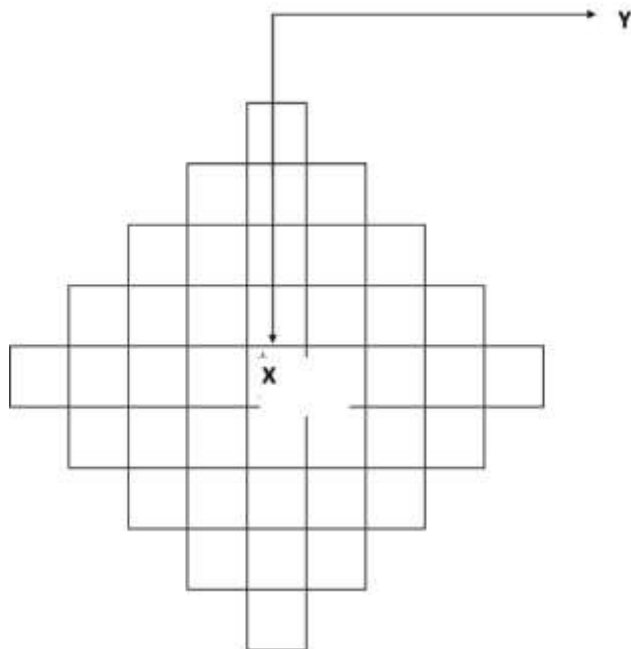


Fig. (1). Representation of the $Z=0$ plane of the lattice used in the calculations.

The clusters of Fig.(2) were then embedded within the central region of the crystal surface. All the electrons of the embedded clusters were included in the Hamiltonian of the *ab initio* calculations. Other crystal sites entered the Hamiltonian either as full or partial ionic charges as demonstrated in Table (1).

Table (1): Specification of the finite lattice used for Flat, Edge, and Br⁻ - corner

surface of KBr. R is half the lattice distance, which for KBr is 3.298Å and r is the distance of the appropriate shell from the center of the lattice.

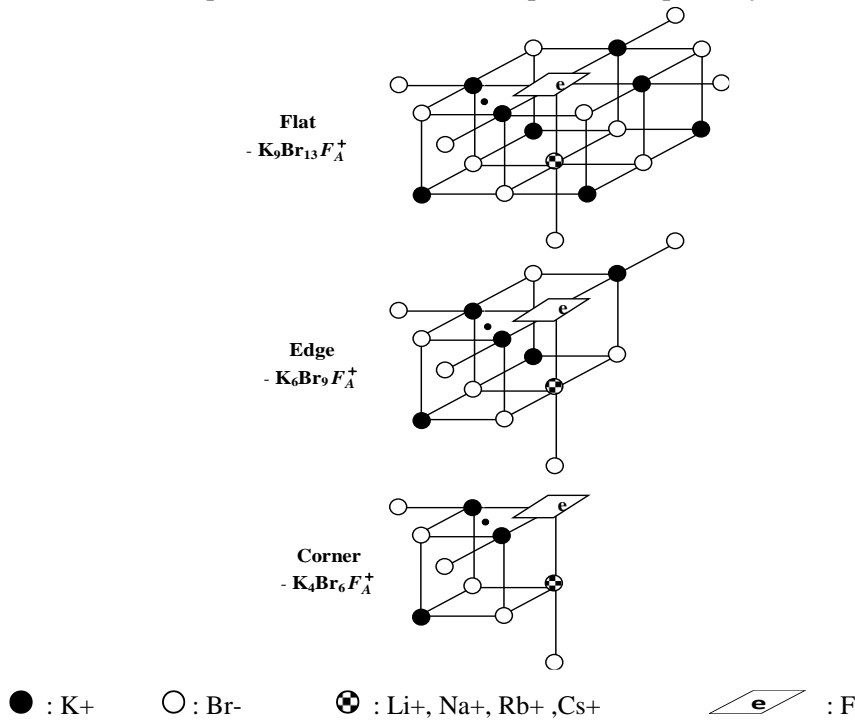
r ² /R ²	Flat		Edge		Br ⁻ - corner		Charge q
	Coordinates/R X , Y , Z	Number of centers	Coordinates/R X , Y , Z	Number of centers	Coordinates/R X , Y , Z	Number of centers	
2	1 1 0	4	1 1 0	4	1 1 0	4	1
6	1 1 2	4	1 1 2	4	1 1 2	4	1
10	3 1 0	8	3 1 0	6	3 1 0	4	1
14	3 1 2	8	3 1 2	6	3 1 2	4	1
18	1 1 4	4	1 1 4	4	1 1 4	4	1
18	3 3 0	4	3 3 0	2	3 3 0	1	1
22	3 3 2	4	3 3 2	2	3 3 2	1	1
26	5 1 0	8	5 1 0	6	5 1 0	4	1
26	3 1 4	8	3 1 4	6	3 1 4	4	1
30	5 1 2	8	5 1 2	6	5 1 2	4	1
32	3 3 4	4	3 3 4	2	3 3 4	1	1
34	5 3 0	8	5 3 0	4	5 3 0	2	1
38	5 3 2	8	5 3 2	4	5 3 2	2	1
38	1 1 6	4	1 1 6	4	1 1 6	4	1
42	5 1 4	8	5 1 4	6	5 1 4	4	1
46	3 1 6	8	3 1 6	6	3 1 6	4	1
50	5 5 0	4	5 5 0	2	5 5 0	1	1
50	5 3 4	8	5 3 4	4	5 3 4	2	1
50	7 1 0	8	7 1 0	6	7 1 0	4	1
54	5 5 2	4	5 5 2	2	5 5 2	1	1
54	3 3 6	4	3 3 6	2	3 3 6	1	1
58	7 3 0	8	7 3 0	4	7 3 0	2	1
66	5 5 4	4	5 5 4	2	5 5 4	1	1
54	7 1 2	8	7 1 2	6	7 1 2	4	0.409283
62	7 3 2	8	7 3 2	4	7 3 2	2	0.409283
66	1 1 8	4	1 1 8	4	1 1 8	4	0.800909
82	9 1 0	8	9 1 0	6	9 1 0	4	0.800909
86	9 1 2	8	9 1 2	6	9 1 2	4	0.800909
		Σ= 176		Σ= 121		Σ= 81	

2.2. Calculations:

2.2.1. Configuration Coordinate Diagrams:

To examine the F_A center tunable laser activity, we have to construct the corresponding configuration coordinate diagrams. In the configuration coordinate diagram[15–18], the electronic energies in the ground and excited states are plotted versus the displacement of usually a single configuration coordinate Q which represents a certain localized mode or normal mode of the lattice coupling

to the electron. In other words, Q represents the simultaneous inward–outward displacements of the nearest neighbor cations to the defect site(s) from the lattice interionic separation ($Q = 0$) along the axes joining them with the defect site(s). The other ions were retained in their original positions in the lattice. Within the harmonic approximation, the electronic states are parabolas with different curvatures for the ground and the excited states and the strength of the electron – phonon coupling is reflected by the different equilibrium positions of the parabolas. For strong coupling the shift is large and for weak coupling it is small. Starting from the doublet ground state of the F_A center an optical excitation produces a transition into the excited states at fixed nuclear coordinates assuming Franck–Condon principle i.e. vertical in the configuration coordinate diagram. Due to the Gaussian shaped probability function for the lowest vibrational state the transition starts with highest probability from the equilibrium position Q_1 . The electronic distribution reached after excitation in the excited state is not in equilibrium with the lattice at Q_1 . As a consequence the ions oscillate towards new equilibrium position. The time needed for this relaxation is in the subpicosecond range [19]. The vibrational energy will be dissipated via anharmonicity into lattice phonons and the electron-lattice system will reach the new equilibrium position Q_2 , the relaxed excited state (RES). After the mean life time the excited electron returns in a vertical emission process to the ground state, and the subsequent lattice relaxation completes the optical cycle [4].



● : 0.0.0

Fig. (2): Representation of the defect containing surfaces of KBr.

The electron–phonon coupling and its effects on the optical transitions can be illustrated with the well-known configuration coordinate diagram. To construct the configuration coordinate diagrams, the ion clusters representing the F_A centers at the flat, edge and corner surfaces of KBr were first embedded in the three-dimensional arrays of point ions described in the Section 2.1. The representation of the ion clusters considered in the calculations is given in Fig. (2). The absorption and emission energies were then calculated as the difference between the total energies of the ground and the excited states. For this purpose, the relevant potential energy curves were calculated, then according to the Franck–Condon principle the absorption energy was calculated as that for a vertical transition from the minimum of the relaxed ground state to the excited state (with fixed atomic coordinates). The luminescence energy was calculated in a similar manner. Stokes shifts were then calculated as the difference between absorption and emission energies.

$$\Delta E_{\text{absorption}} - \Delta E_{\text{emission}} \quad (1)$$

2.2.2. Configuration interaction-singles method.

The configuration interaction-singles(CIS) method was employed for the calculations of F_A tunable laser activity, exciton (energy) transfer, relaxed excited state orientational bleaching and defect formation energies. The full CI method forms the wavefunction Ψ as a linear combination of the Hartree–Fock determinant and all possible substituted determinants:

$$\Psi = b_0 \Psi_0 + \sum_{s>0} b_s \Psi_s \quad (2)$$

where the 0 indexed term is the Hartree–Fock level, and s runs over all possible substitutions. In a single substitution, a virtual orbital replaces an occupied orbital within the determinant. The b_s are the set of coefficients to be solved for by minimizing the energy of the resultant wavefunction. Consequently, the Configuration Interaction-Singles method uses the configuration interaction approach and models excited states as combinations of single substitutions out of the Hartree–Fock ground state. The CI-Singles theory is an adequate zeroth-order treatment for many excited states of molecules. Treatments of large molecular systems can be made affordable by the avoidance of integral storage and transformation, and thus the Configuration Interaction-Singles method has a wide range of applicability. A satisfactory exploration of potential energy surfaces and accurate electronic properties of excited states are possible by the

use of an analytic Configuration Interaction-Singles gradient [20a]. The method includes some electron correlation in the excited states, and can provide reasonable accuracy for excitation energies in comparison with the simplest way to find the lowest relaxed excited state in wide gap insulators, namely, the self consistent field calculations of the triplet state [21]. We also note that Sousa and Illas [20b] have examined the impact that proper electron correlation treatment could have an optical absorption energy of F -centers in MgO.

2.2.3. Density functional theory method.

Density functional theory method was employed for the calculations of the differences between the band gaps and exciton bands (Glasner–Tompkins relation). Kohn and Sham [20c] showed that the exact ground-state purely electronic energy E of an n -electron molecule with ground state electron probability density ρ is given by the equation

$$E = -1/2 \sum_{i=1}^n \langle \Psi_i(1) | \nabla_i^2 | \Psi_i(1) \rangle - \sum_{\alpha} \frac{Z_{\alpha} \rho(1)}{r_{1\alpha}} dv_1 + 1/2 \iint \frac{\rho(1)\rho(2)}{r_{12}} dv_1 dv_2 + E_{XC}[\rho] \quad (3)$$

where Ψ_i , $i = 1, 2, \dots, n$ are the Kohn–Sham orbitals, and the exchange correlation energy $E_{XC}[\rho]$ is a functional in ρ . Kohn and Sham also showed that the exact ground-state ρ can be found from Ψ_i 's, according to

$$\rho = \sum_{i=1}^n |\Psi_i|^2 \quad (4)$$

The density functional theory calculations were performed by using Becke's three-parameter exchange functional B3 with LYP correlation functional [22]. This hybrid functional includes a mixture of a Hartree–Fock exchange with DFT exchange correlation. Originally the functional B included the Slater exchange along with corrections involving the gradient of the density [23] and the correlation functional LYP is that of Lee, Yang and Parr, which includes both local and non-local terms [24].

The adsorption energy E_{ads} of the adatom on the substrate surface was calculated from the relation

$$E_{ads} = E_{complex} - E_{adsorbte} - E_{substrate} \quad (5)$$

The terms appearing on the right hand side are the total energies of the complex (adsorbate + substrate), the adsorbate (F; Cl; Br; I; At) and the substrate (defect-free or defect containing), obtained from three independent calculations using the same supercell. The negative adsorption energy E_{ads} indicates that the bound adsorbate is electronically stable. Stevens and coworkers ECP basis set CEP-121G [25] was employed in the calculations.

The computations reported in this paper were carried out by using Gaussian 98 system [26].

3. Results and Discussion:

3.1. F_A laser and related properties

3.1.1. F_A tunable laser activities

The configuration coordinate data of F_A at the low coordinated surfaces of KBr are given in Table (2) and the configuration coordinate curves are given in Fig. (3a, b, c, d). The strength of the electron– phonon couplings as reflected by the shifts in the equilibrium positions $Q_2 - Q_1$ and the values of Stokes-shifts between the ground states and the low lying excited states follow the order flat > edge > corner for L_i^+ , N_a^+ and R_b^+ . In case of C_s^+ follow the order edge > corner > flat. In the other words of cationic radius ($L_i^+ > N_a^+ > R_b^+ > C_s^+$) for flat and corner and ($L_i^+ > N_a^+ > C_s^+ > R_b^+$) for edge. The laser activity attributed to the F_A centers at the (0 0 1) surface of KBr crystal is therefore inversely proportional to the size of the dopant cation (L_i^+ , N_a^+ , R_b^+ , C_s^+) relative to the size of the host cation (K^+).

Table (2): Minima of the ground states (Q_1), low lying excited states (Q_2), horizontal shifts along the configurations coordinate (Q_2-Q_1), absorption and emission energies $E_{absorption}$ and $E_{emission}$ and Stokes - shifts of F_A centers at the low coordinated surfaces of KBr calculated at the CIS level. All lengths are given in Å and energies are given in eV.

	Q_1	Q_2	$Q_2 - Q_1$	$E_{absorption}$	$E_{emission}$	Stokes - shifts
<i>Flat</i>						
Li^+	3.56	3.73	0.17	0.984	0.464	0.520
Na^+	3.55	3.71	0.16	1.039	0.528	0.511
Rb^+	3.55	3.68	0.13	0.989	0.599	0.390
Cs^+	3.49	3.55	0.06	1.092	0.926	0.166
<i>Edge</i>						
Li^+	3.53	3.73	0.20	1.054	0.618	0.436
Na^+	3.55	3.71	0.16	1.016	0.641	0.375
Rb^+	3.55	3.68	0.13	0.972	0.681	0.291
Cs^+	3.46	3.61	0.15	1.089	0.772	0.317
<i>Corner</i>						

Li ⁺	3.50	3.74	0.25	1.170	0.871	0.300
Na ⁺	3.55	3.73	0.18	0.968	0.690	0.278
Rb ⁺	3.56	3.69	0.13	0.777	0.552	0.225
Cs ⁺	3.45	3.56	0.11	0.823	0.620	0.203

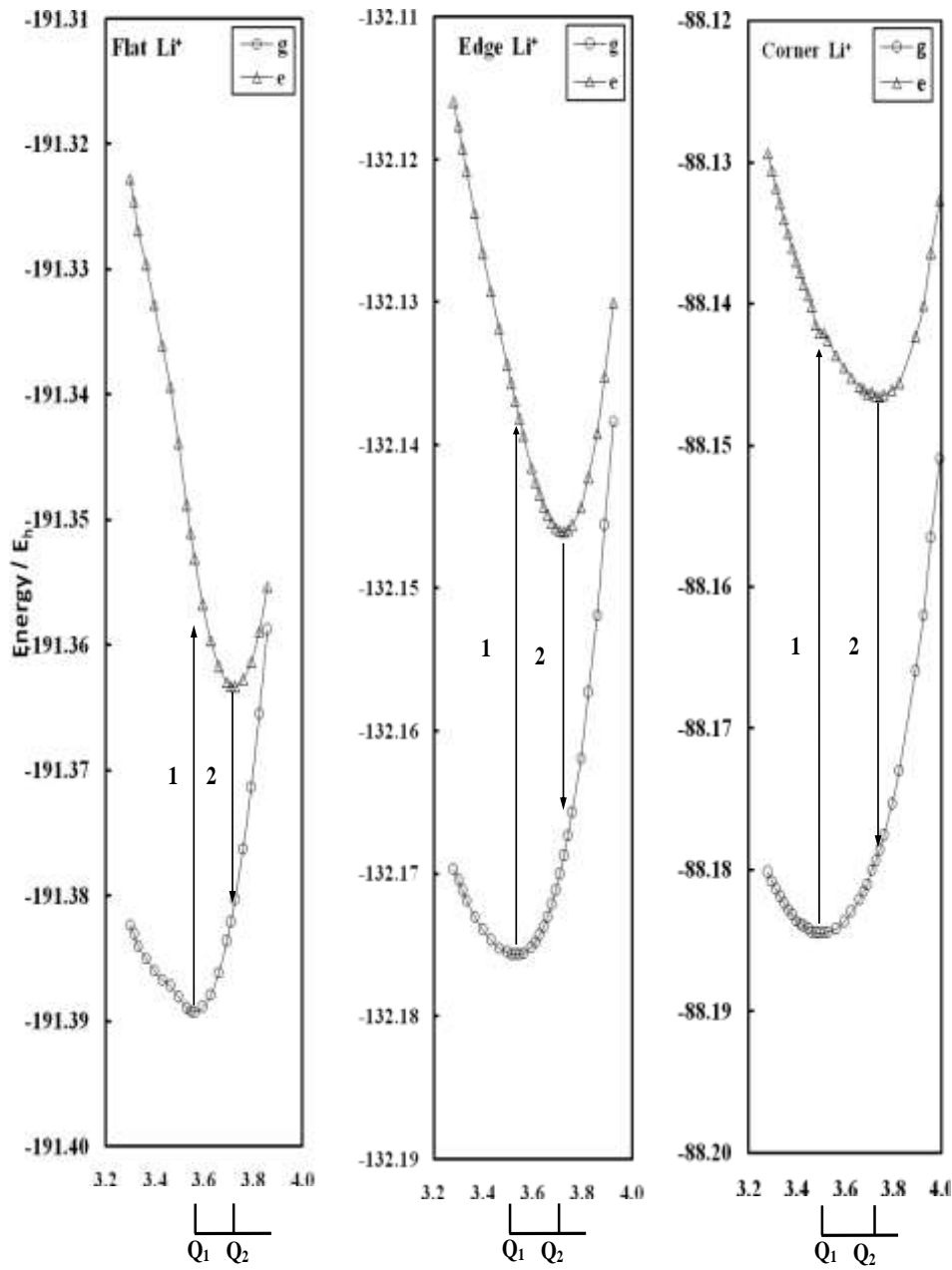


Fig. (3a): The configuration coordinates diagrams of the low coordinated surfaces of KBr with F_A color center. Minima of the ground states (Q_1) and low lying excited states (Q_2).
g: ground stat e: low lying excited state 1: absorbtion 2: emission

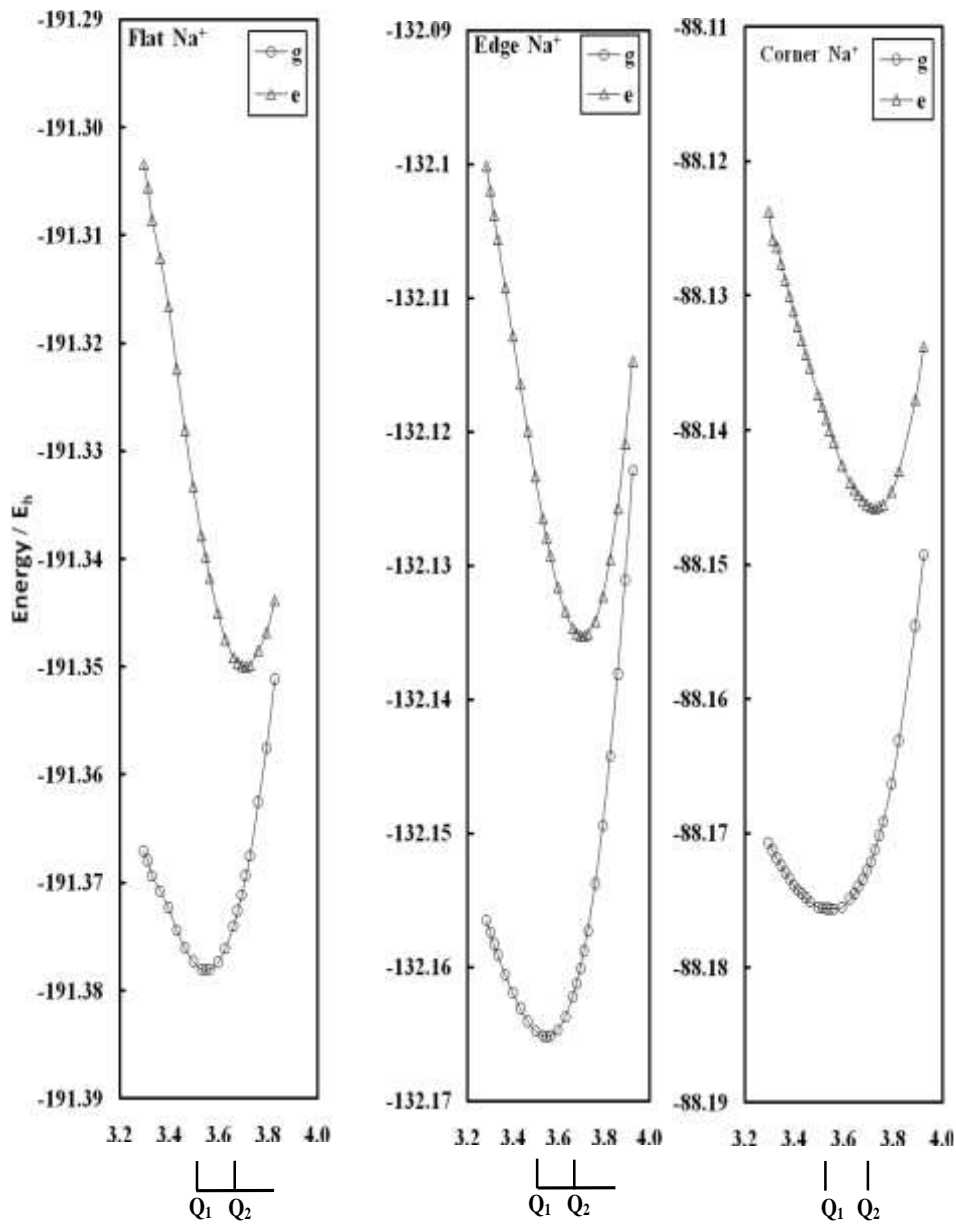


Fig. (3b): The configuration coordinates diagrams of the low coordinated surfaces of KBr with F_A color center. Minima of the ground states (Q_1) and low lying excited states (Q_2).

g: ground state e: low lying excited state 1: absorption 2: emission

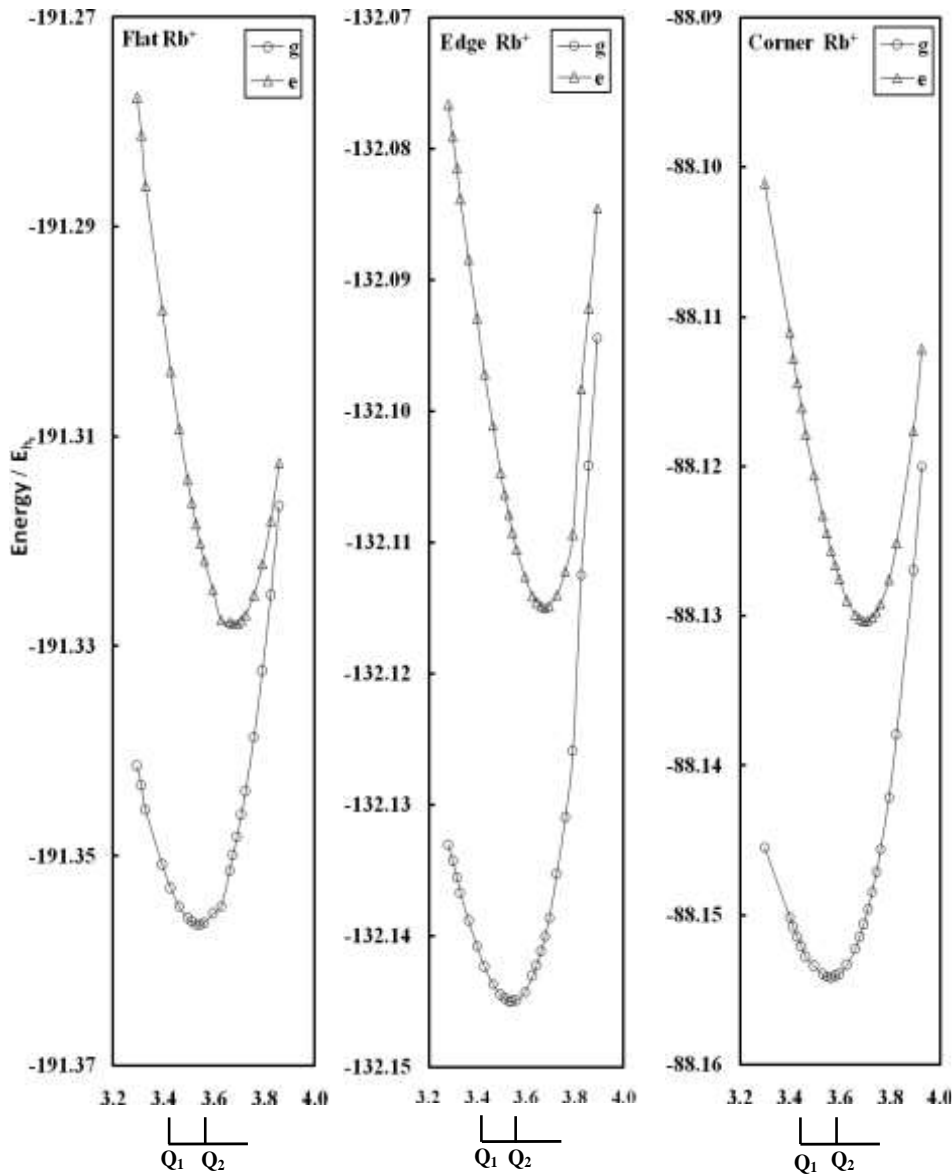


Fig. (3c): The configuration coordinates diagrams of the low coordinated surfaces of KBr with F_A color center. Minima of the ground states (Q_1) and low lying excited states (Q_2).

g: ground stat e: low lying excited state 1: absorption 2: emission

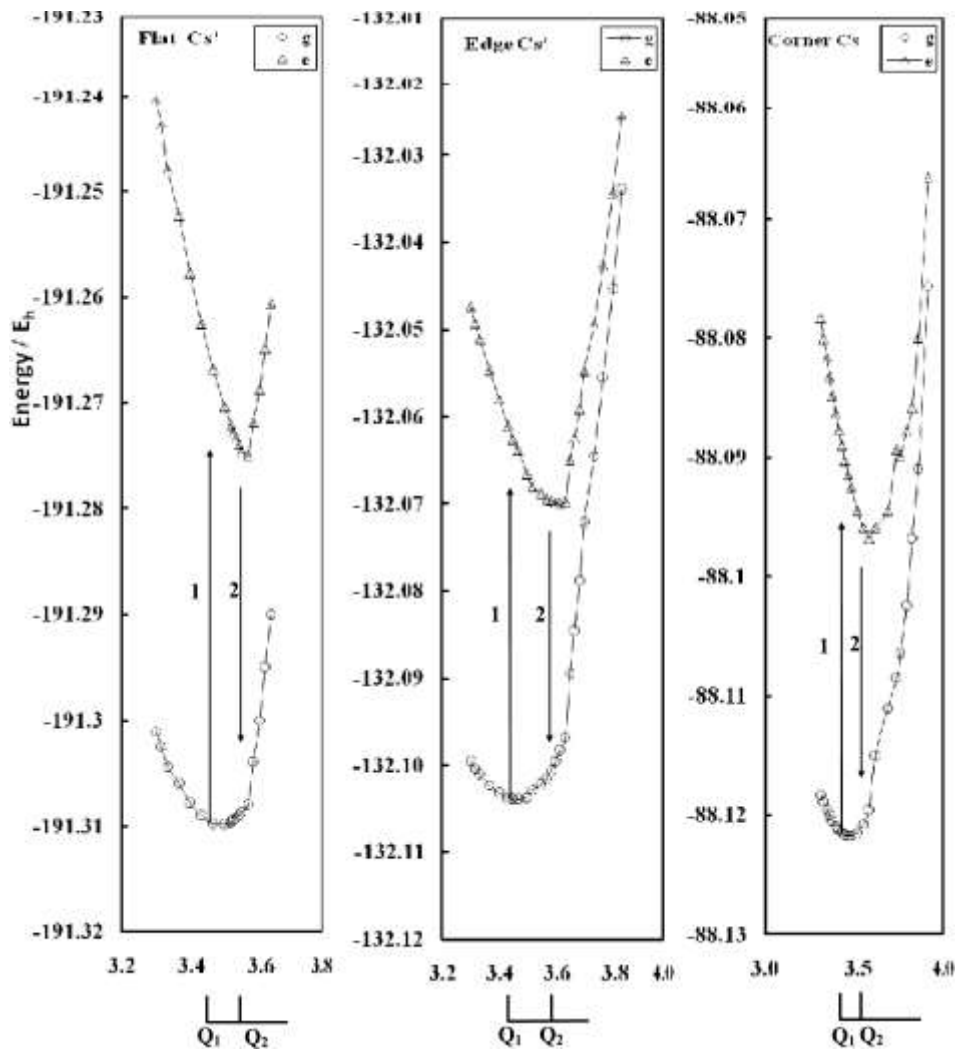


Fig. (3d): The configuration coordinates diagrams of the low coordinated surfaces of KBr with F_A color center. Minima of the ground states (Q_1) and low lying excited states (Q_2).
 g: ground stat e: low lying excited state 1: absorbtion 2: emission

To explain this relation, consider the present type I F_A (F centers attached to the large-size cationic impurities R_b^+ and C_s^+ relative to K^+) and type II F_A centers (F centers attached to the small-size cationic impurities L_i^+ and N_a^+ relative to K^+). In type I F_A centers, the anisotropy and np splitting observed in absorption disappears in the relaxation process; the wave function of the relaxed excited state RES is spatially diffused, the ns states lie below the

np states and a depolarized long lifetime emission results, similar to the F centers case, including small Stokes shifts relative to that of K^+ . The only difference in the emission process is a slightly higher transition probability due to the axial perturbation of the impurity ion. In type II F_A centers, the splitting of the absorption transitions is similar to the type I F_A case but the relaxation process is drastically changed. Due to the small size of the neighboring impurity relative to K^+ , the system minimizes its energy by relaxing into an 'ionic saddle point configuration', forming a double well potential for the center electron in the relaxed excited state. The lowest electronic states of this potential are symmetric and antisymmetric combinations of the ground states of the two wells. They have an energy separation and are connected by strongly allowed electric dipole transitions. As a result, type II F_A centers show a polarized emission with large radiative transition probability and Stokes shifts relative to K^+ . This leads to a two-fold increase in the cross-section for stimulated emission as compared with type I F_A centers.

3.1.2. Relaxed excited state orientational bleaching

One consequence of the relaxed excited state saddle point configuration of F_A center is a temperature independent ionic reorientation during the pump cycle, i.e. a change of the center axis into a perpendicular (equivalent) orientation. This effect can be understood from Fig. (4) where it is seen that after the emission process the saddle point ion has a 50% chance of hopping to the $\langle 110 \rangle$ anion vacancy site opposite to its starting location. Therefore, if an F_A center system, in particular type II F_A , is excited in either one of its absorption bands with polarized light having its propagation direction parallel to a $\langle 100 \rangle$ axis and the electric field vector E parallel to a perpendicular $\langle 100 \rangle$ axis, the F_A centers excited by the E -vector will quickly switch to $\langle 100 \rangle$ directions where they are no longer excited and the system will become experimentally transparent for the excitation light [4]. To examine the orientational bleaching theoretically, we have calculated the total energies of the original relaxed excited state configurations and the assumed relaxed excited state saddle point configurations of type I and II F_A centers at the surface of KBr. The differences between the energies of these configurations (the energy barriers to orientational bleaching in laser experiment) are given in Table (3), from which it is shown that the barrier to the migration of bromide anion F_A site is directly proportional to the size of the dopant cation. We may therefore conclude that the probability of orientational bleaching is inversely proportional to the size of the impurity cation relative to the host cation. In other words, orientational bleaching can occur in both types of F centers (I and II) but more probable for type II than for type I. Experimentally, in order to avoid orientational bleaching, the pump polarization and direction of

propagation of the pump beam inside the crystal have to be chosen such that they are not parallel to a $\langle 100 \rangle$ direction.

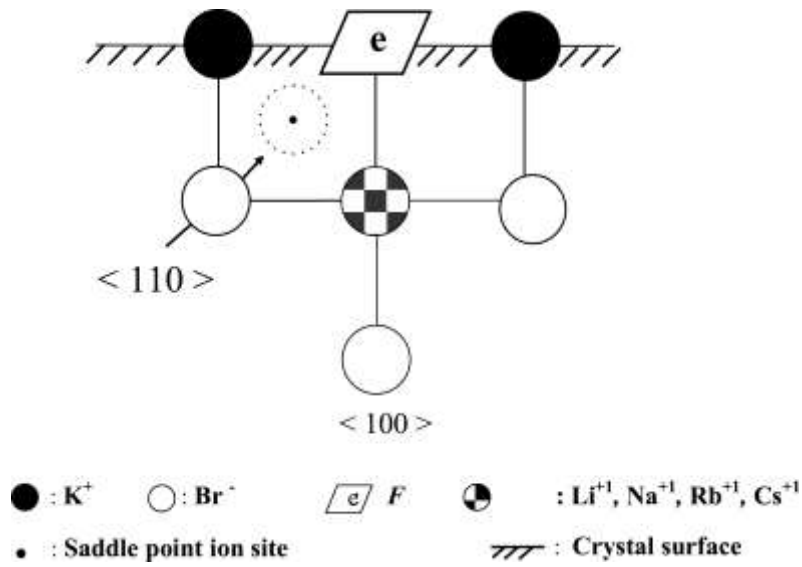


Fig. (4): Representation of the assumed RES saddle point ion configurations responsible for orientational bleaching in laser experiment.

Table (3): Energy barriers to orientational bleaching of F_A center at the low coordination surfaces of KBr.

<i>Flat</i>		
	Li⁺	0.511
	Na⁺	0.868
	Rb⁺	1.421
	Cs⁺	1.600
<i>Edge</i>		
	Li⁺	1.276
	Na⁺	1.613
	Rb⁺	2.026
	Cs⁺	2.882
<i>Corner</i>		
	Li⁺	0.039
	Na⁺	2.200
	Rb⁺	2.060
	Cs⁺	3.275

^a Energies are given in eV.

3.1.3. Exciton (energy) transfer

The relative total energies of the excited states at different low coordinated surface sites could be used as the first indicator of whether the exciton excited at a particular surface site would transfer to another site. In order to be able to compare the results for different shapes and sizes of quantum clusters, the relative energies of the excited states for different coordinations were estimated following the method of Shluger et al [22]. The ionization energies I for the clusters were calculated using the CIS method. Assuming the vacuum level for all systems considered, the ground state total energies were placed at $-I$ as shown in Fig (5). Then the energies of the excited states were located with respect to the defined positions of the ground states using the excitation energies. As one case see in Fig 5, the excited states at the corner has higher energy than that at the flat or at the edge surfaces. The energies of the excited states at the edge and corner surface appear to be very similar.

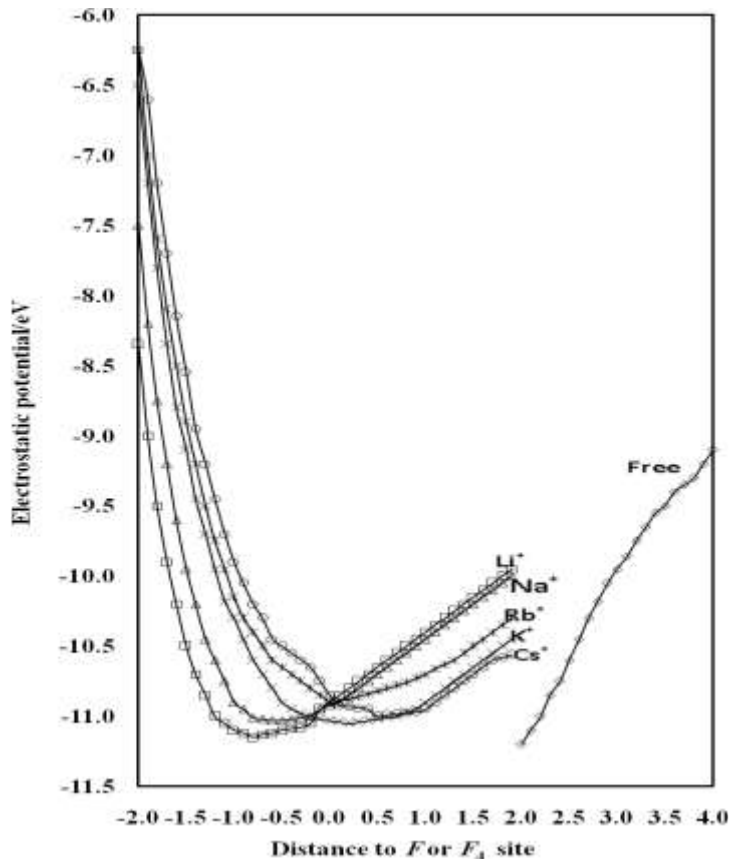


Fig. (5): Electrostatic potential curves over the defect- free and defect containing surfaces of KBr.

3.1.4. F_A defect formation energies

To clarify the dependence of F_A defect formation energies on the bromide ion coordination, an attempt has been made to calculate this quantity at each of the flat, edge and corner sites. The F_A defect formation energies were calculated by subtracting the sum of the total energies of the reactants from those of the products

$$E_{formation} = E_{products} - E_{reactants} \quad (6)$$

Here the reactants are the defect-free flat, edge and corner surfaces and the products are the corresponding defect-containing surfaces as well as the free Br atom and K^+ ion. The defect formation energies are given in Table (4). As one can see in this table, F_A defect can be easily formed at the low coordinated corner surface relative to the flat and edge surfaces. In other words, we can conclude that the products of type II F_A center can be easily formed relative to I F_A .

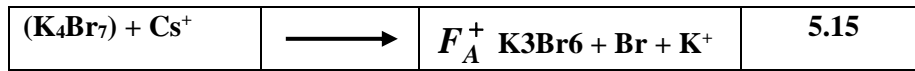
3.1.5. The Glasner – Tompkins relation

Glasner and Tompkins [27] reported an empirical relationship between the principal optical absorption of F -centers in solids and the fundamental absorption of the host crystal. The difference between the first exciton absorption energy E_X and the F band energy E_F was found to depend almost exclusively on the negative ion species. In other words, the Glasner–Tompkins empirical rule suggests that the energy difference between the fundamental absorption of an alkali halide and the F band is very nearly a function of the halide species alone. E_X , E_F , $E_X - E_F$ and $\langle E_X - E_F \rangle$ for twelve alkali halides have been reported by Malghani and Smith [28], and for LiH and LiF by Shalabi et al. [29]. To apply the Glasner–Tompkins relation to the present F and F_A center at the low coordinated surfaces of KBr, the bromide ion coordination dependence of band gaps and exciton bands is needed. A complete treatment for understanding the host dependence of band gaps would involve theories of excitons [30] and defects [31] which take into account the band structure. We use the simple electron transfer model of the fundamental optical absorption of ionic solids developed by Hilsch and Pohl [32]. This model, in its simplest form, explains the fundamental optical absorption E_X as the transfer of an electron from a negative ion to a neighboring positive ion both placed adjacent to the defect site. It seems likely that all centers have perturbed excitons formed nearby [17, 33-34]. Theoretically, we calculate E_X as the change in Coulomb energy associated with the transfer of an electron from a

halide host ion to an alkali host ion, both placed adjacent to the F or F_A center, and calculate E_F as the energy gap between the valence and conduction bands. The correlation between the bromide ion coordination and the energy difference between the exciton bands and band gaps, E_x and E_F , respectively are given in Table (5). As shown, the results emphasize the exclusive dependence of the energy differences on the bromine coordination. The energy difference is significantly reduced as the bromine coordination increases, generalizing in turn, the Glasner–Tompkins relation to include the reduced bromine coordination at KBr surface

Table (4) : The defect formation energies at the low coordination surfaces of KBr^a.

<i>Flat</i>			
(K₉Br₁₄) + Li⁺	————→	F_A^+ K₈Br₁₃ + Br + K⁺	4.11
(K₉Br₁₄) + Na⁺	————→	F_A^+ K₈Br₁₃ + Br + K⁺	4.44
(K₉Br₁₄)	————→	F_A^+ K₉Br₁₃ + Br	5.19
(K₉Br₁₄) + Rb⁺	————→	F_A^+ K₈Br₁₃ + Br + K⁺	6.36
(K₉Br₁₄) + Cs⁺	————→	F_A^+ K₈Br₁₃ + Br + K⁺	5.44
<i>Edge</i>			
(K₆Br₁₀) + Li⁺	————→	F_A^+ K₅Br₉ + Br + K⁺	4.16
(K₆Br₁₀) + Na⁺	————→	F_A^+ K₆Br₉ + Br + K⁺	4.47
(K₆Br₁₀)	————→	F_A^+ K₅Br₉ + Br	5.16
(K₆Br₁₀) + Rb⁺	————→	F_A^+ K₅Br₉ + Br + K⁺	6.17
(K₆Br₁₀) + Cs⁺	————→	F_A^+ K₅Br₉ + Br + K⁺	5.33
<i>Corner</i>			
(K₄Br₇) + Li⁺	————→	F_A^+ K₃Br₆ + Br + K⁺	3.89
(K₄Br₇) + Na⁺	————→	F_A^+ K₃Br₆ + Br + K⁺	4.26
(K₄Br₇)	————→	F_A^+ K₄Br₆ + Br + K⁺	5.05
(K₄Br₇) + Rb⁺	————→	F_A^+ K₃Br₆ + Br + K⁺	5.88



^a Energies are given in eV.

Table (5): F_A band gaps E_{FA} and exciton bands E_X of the defect containing surfaces of KBr.^a

	E_{FA}^+	E_X	$E_X - E_{FA}^+$
Flat			
Li ⁺	1.205	10.676	9.471
Na ⁺	1.193	10.684	9.491
K ⁺	1.102	10.698	9.596
Rb ⁺	1.129	10.699	9.570
Cs ⁺	1.042	10.700	9.658
Edge			
Li ⁺	1.184	10.777	9.593
Na ⁺	1.160	10.786	9.626
K ⁺	1.094	10.802	9.708
Rb ⁺	1.111	10.802	9.691
Cs ⁺	1.040	10.808	9.768
Corner			
Li ⁺	1.472	10.735	9.263
Na ⁺	1.280	10.732	9.452
K ⁺	0.959	10.702	9.743
Rb ⁺	0.960	10.701	9.741
Cs ⁺	0.764	10.691	9.927

^a Energies are given in eV.

3.2. The adsorptivity of halogen atoms

3.2.1. Electrostatic potentials

To shed light on the possible electrostatic contributions to the adsorbate–substrate interactions when using the defect-free and defect containing surfaces of KBr, we looked first at the electrostatic potential curves at the bromide ion site of the defect-free surface and the F and F_A sites of the defect containing surfaces. Fig. (6) shows that the electrostatic potentials due to the defect-free and defect containing surfaces are different at the distances considered for adsorbate–substrate interactions, leading thus to different electric fields and electric field derivatives. Since the electrostatic interaction of the adatom with the surface will mainly consist of electric field induced dipole and electric field derivatives-induced quadrupole moments, one expects that the classical

contributions to the adsorbate–substrate interactions are quite different for the defect-free and the defect containing surfaces of KBr (see Fig. 7).

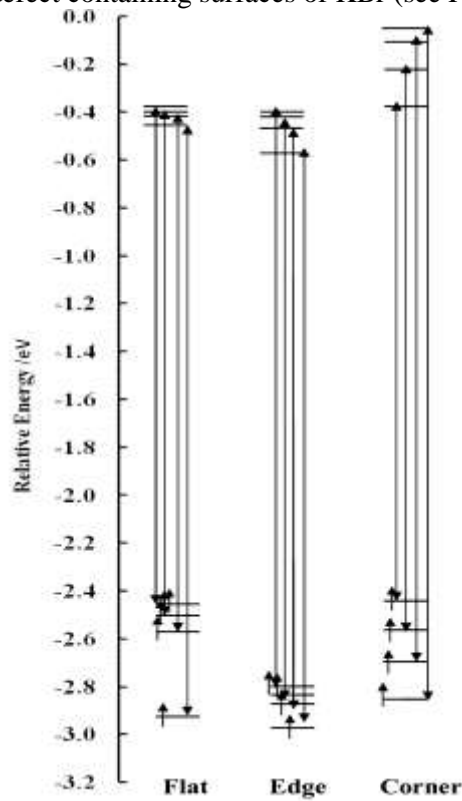


Fig. (6): Diagram representing the relative energies of ground and excited states of the low coordinated surfaces of KBr.

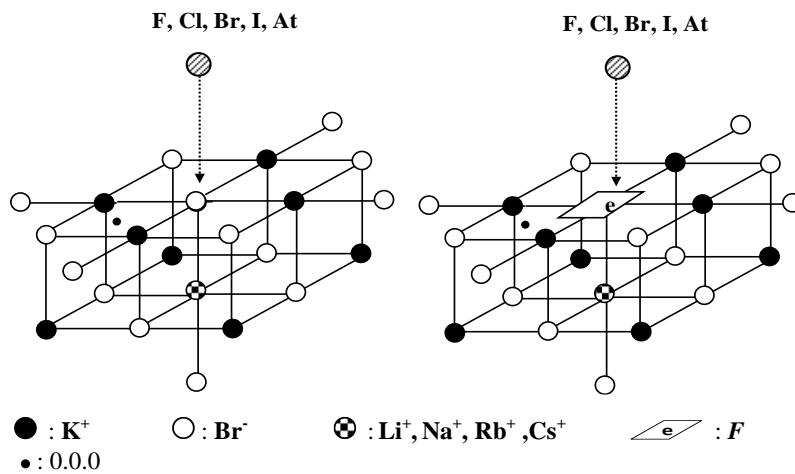


Fig. (7): The adsorption of the F, Cl, Br, I and At over the defect-free and defect containing surfaces of KBr.

3.2.2. The adsorbate – substrate interactions

We may now consider the adsorbate–substrate interactions by examining the adsorptivity of F, Cl, Br, I and At on two equivalent sites, namely the bromide ion site of the defect-free surface and the F and F_A sites of the defect containing surfaces. The ions surrounding the F or F_A center were allowed to relax to equilibrium and the adsorbate–substrate distances were optimized in all cases. The corresponding results of the equilibrium adsorbate–substrate distances and adsorption energies are collected in Table 6. As shown in Table 6, the halogen atoms adsorb chemically under the effect of F or F_A center imperfection. The F or F_A surface imperfection enhances the adsorption of the halogen atoms and change the nature of adsorption from physical adsorption to chemical adsorption. The type I F_A center enhances the adsorption of the halogen atoms more significantly than the F and II F_A centers and the adsorption energies are monotonically increasing function in the electronegativity of the halogen species. The calculated pattern of adsorption energies is consistent with that already expected from the electrostatic potential curves where distinct differences in adsorption energies occur between the defect-free and the defect containing surfaces.

3.2.3. Mulliken charges and adsorbate – substrate interactions

To correlate the strength of halogen interactions at the considered surface sites with the electronic charge distribution, using Mulliken method of population analysis, we collected the charges on the adsorbed halogen atom in each complex in Table (7). As shown, the strength of adsorbate – substrate interaction (the adsorption energy) is directly proportional to the amount of charge transferred between the halogen atom and the defect-free surface. With some exceptions (Cl and Br adsorbates), the strength of adsorbate – substrate interaction is also shown to be directly proportional to the amount of charge transferred between the halogen atom and the defect containing surfaces. One may therefore expect that spin pairing between the open shell adsorbate and substrate surface plays an important role in the adsorptivity of halogen atoms at the KBr surface.

3.2.4. The relative roles of energy gaps and spin pairing.

To examine the relative roles of (i) the energy gap between the halogen atom and the substrate surface, (ii) the spin pairing between the halogen atom single electron and the F or F_A single electron, in the course of the adsorbate–substrate interactions, the energy levels, tops of valence bands and bottoms of conduction bands for each of the F, Cl, Br, I and At as well as the defect-free

and the defect containing surfaces are given in Fig. (8). We first know from Table (7) that the adsorptivity of the halogen atoms follows the order $F > Cl > Br > I > At$. Inspection of Fig. (8) shows that the energy gaps between the halogen atoms and the substrate surface follows unexpectedly the same order. We have therefore state that the spin pairing factor, rather than the energy gap factor, plays the dominant role in the course of adsorbate–substrate interactions and the large increase in adsorption energies, following surface imperfection, is mainly attributed to the role of spin pairing.

Table(7) : Mulliken charges of F, Cl, Br, I and At adsorbates over the defect free and defect containing surfaces of KBr.

	F	Cl	Br	I	At
KBr	-0.2754	-0.2561	-0.2066	-0.1694	-0.1504
$F_A : Li^+$	-0.7379	-0.7785	-0.7819	-0.7237	-0.6425
$F_A : Na^+$	-0.7402	-0.8003	-0.8160	-0.7805	-0.7235
$F : K^+$	-0.7569	-0.8236	-0.8409	-0.7830	-0.7445
$F_A : Rb^+$	-0.8300	-0.8409	-0.8492	0.7806	-0.7352
$F_A : Cs^+$	-0.8210	-0.8394	-0.8460	-0.7860	-0.7400

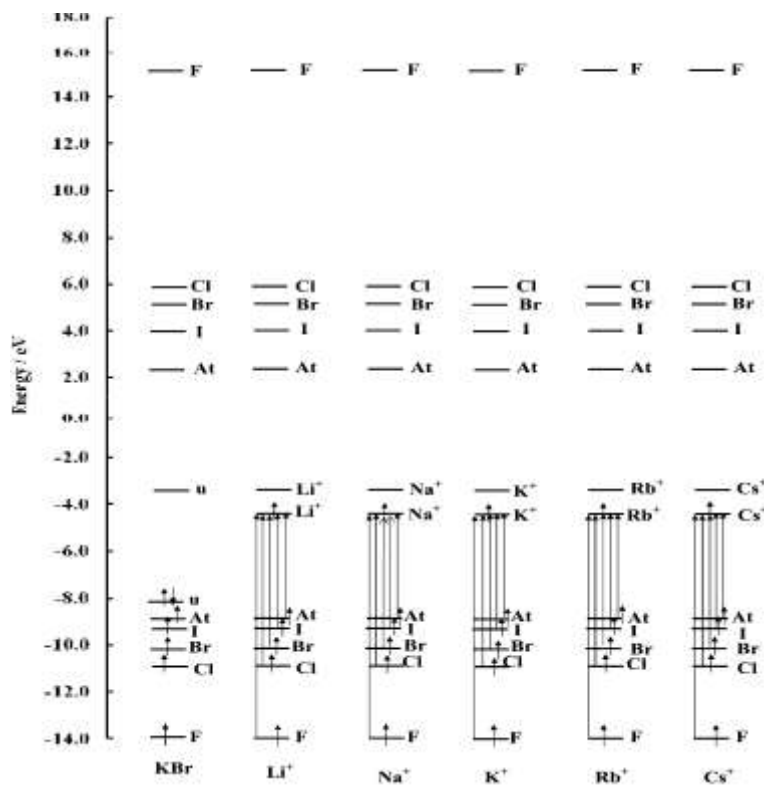


Fig. (8): The energy levels, tops of valence bands and bottoms of the conduction bands for F, Cl, Br, I, At, defect free and the defect containing surfaces of KBr

3.2.5. Band gaps and electrical conductivity

Fig.(8) shows that the defect-free surface of KBr can be made semiconducting by F and $F_A(L_i^+, N_a^+, R_b^+, C_s^+)$ centers. The band gap of the defect-free surface was significantly reduced to less than 2 eV (the domain of band gaps of a semiconducting material is ≤ 2 eV). This in turn implies that the electrical conductivity of an insulator can be significantly enhanced under the effect of electrons trapped in holes.

4. Conclusions

Ab initio molecular electronic structure calculations have been carried out to examine the F_A center tunable laser activity color centers and adsorptivity of halogen atoms (F, Cl, Br, I, At) at the low-coordination (100) surface sites of KBr. Two commonly used methods, CIS and DFT, have been employed, and quantum clusters have been embedded in the simulated Coulomb fields of the crystal surfaces. The considered F_A color centers were found to be suitable laser defects, and the laser activity was found to be inversely proportional to the size of the dopant cation ($L_i^+, N_a^+, R_b^+, C_s^+$) relative to the host cation (K^+). In other words they decreases significantly as the bromine coordination decreases from 5 (flat) to 4 (edge) to 3 (B_r^- corner). The probability of orientational bleaching attributed to the RES saddle point ion configuration along the (110) axis was found to be inversely proportional to the size of the dopant cation. The excited state at the corner has higher energy than that at the flat or at the edge surfaces. The Glasner–Tompkins relation is generalized to include the reduced bromine coordination at the KBr surfaces. The F or F_A surface imperfections enhance the adsorption of the halogen atoms and change the nature of adsorption from physical adsorption to chemical adsorption. The spin pairing mechanism played the dominant role in the course of adsorbate–substrate interactions and the KBr defect free surface can be made semiconducting by F or $F_A(L_i^+, N_a^+, R_b^+, C_s^+)$ surface imperfections.

References:

1. B. Fritz, E. Menke, *Soild State Commun.* **3**, 61, (1965).
2. L.F. Mollenauer, D.H. Olson, *Appl. Phys. Lett.* **24**, 386, (1974).
3. F. Luty, *Physics of Color Centers*, ed. W. B. Fowler, Academic Press, New York, ch., 3 (1968).
4. W. aGellermann, *J. Phys. Chem. Solids*, **52**, 249, (1991).

5. J.J. Markham, F centers in Alkali Halides, Academic Press, New York, (1966).
6. S. Coluccia, L. Marchese, in: K. Tanabe, H. Hattori, T. Yamaguchi, T. Tanaka (Eds.), International Symp. on Acid–base Catalysis, Kodansha, Tokyo, (1988).
7. H.M. Evjen, *Phys. Rev.* **39**, 675, (1932).
8. E. A. Colbourn and W. C. Mackrodt, *Surf. Sci.*, **117**, 571, (1982).
9. Z. Barandiaran and L. Seijo, *J. Chem. Phys.*, **89**, 5739,(1988);
10. Z. Barandiaran and L. Seijo, in Computational Chemistry:Structure, Interactions and Reactivity, Vol.77B of Studies in Physical and Theoretical Chemistry, ed. S. Fraga, Elsevier, Amsterdam, pp. 435 (1992).
11. E. A. Colbourn, in Advances in Solid State Chemistry, ed. C. R. A. Catlow, JAI Press, London, vol. I (1999).
12. A.S. Shalabi, A.M. El-Mahdy, *J. Phys. Chem. Solids*, **60**, 305, (1999).
13. A.S. Shalabi, S. Abdel Aal, M.A. Kamel, H.O. Taha, H.Y. Ammar, W.S.Abdel Halim, *Chem. Phys.* **328**, 8, (2006).
14. A.S. Shalabi, S. Abdel Aal, M.A. Kamel, H.O. Taha, W.S. Abdel Halim, *Physica*, B **387**, 6, (2007).
15. A.S. Shalabi, *J. Mol. Model*, **8**, 1104 (2002).
16. G.W. Hills, *Opt. Commun.* **42**, 360, (1982); W. Gellwerman, F. Ly, C.R. Pollock, *Opt. Commun.* **39**, 391 (1981); C. Domene, P.W. Fowler, M. Wilson, P.A. Madden, R.J. Wheatley, *Chem. Phys. Lett.* **333**, 403 (2001); A.S. Shalabi, S. Abdel Aal, W.S. Abdel Halim, H.Y. Ammar, *J. Mol. Struct. Theochem.* **823**, 47, (2007).
17. S. Coluccia, L. Marchese, in: K. Tanabe, H. Hattori, T. Yamaguchi, T. Tanaka (Eds.), International Symposium on Acid–Base Catalysis, Kodansha, Tokyo, 1988; G.T. Surrat, A.B. Kunz, *Phys. Rev. Lett.* **40**, 347, (1978); E.A. Colbourn, *Surf. Sci. Rep.* **15**, 281, (1992).
18. A.S. Shalabi, A.M. El-Mahdy, M.A. Kamel, H.Y. Ammar, *Physica*, B **292**, 59,(2000); A.S. Shalabi, A.M. El-Mahdy, M.A. Kamel, G.H. Ismail, *J. Phys. Chem. Solids*, **60**, 1007, (2001).
19. W.B. Fowler, D.L. Dexter, *Chem. Phys.* **43**, 768, (1965).
20. J. Wiesenfield, L.F. Mollenauer, E. Ippen, *Phys. Rev. Lett.* **47**, 1668, (1981).
21. J.B. Foresman, M. Head-Gordon, J.A. Pople, M.J. Frisch, *J. Phys. Chem.* **96**, 135, (1992); J.B. Foresman, J.B. Foresman, Exploring chemistry with electronic structure methods, second ed., Gaussian Inc., Pittsburgh, PA, 1996;(b) C. Sousa, F. Illas, *J. Chem. Phys.* **115**, 1435, (2001); (c) W. Kohn, L.J. Sham, *Phys. Rev. A* **140**, 1133,(1965).
22. A.L. Shluger, P.V. Sushko, L.N. Kantorovich, *Phys. Rev. B* **59**, 2417,(1999).

23. A.D. Becke, *J. Chem. Phys.* **98**, 5648, (1993).
24. A.D. Becke, *Phys. Rev. A* **38**, 3098, (1988).
25. C. Lee, W. Yang, R.G. Parr, *Phys. Rev. B* **37**, 785, (1988); B. Miehlich, A. Savin, H. Stoll, H. Preuss, *Chem. Phys. Lett.* **157**, 200 (1989).
26. W. Stevens, M. Krauss, H. Basch, P.G. Jasien, *Can. J. Chem.* **70**, 612, (1992); T.R. Cundari, W.J. Stevens, *J. Chem. Phys.* **98**, 5555 (1993).
27. W. Stevens, H. Basch, J. Krauss, *J. Chem. Phys.* **81**, 6026, (1984);
28. M.J. Frisch, et al., Gaussian 98, Gaussian, Inc., Pittsburgh, PA, (1998).
- A. Glasner, F.C. Tompkins, *J. Chem. Phys.*, **21**, 1817, (1953).
29. M.S. Malghani, D.Y. Smith, *Bull. Am. Phys. Soc.*, **36**, 1681 (1991).
30. M.S. Malghani, D.Y. Smith, *J. Phys. Chem. Solids*, **53**, 831 (1992).
31. A.S. Shalabi, A.M. El-Mahdy, Kh.M. Eid, M.A. Kamel, A.A. El-Barbary, *Phys. Rev. B* **60**, 9377, (1999).
32. R.S. Knox, Theory of Excitons, Academic Press, New York, (1963); V.G. Plekhanov, *Phys. Rev. B* **54**, 3869,(1996); A.A.O. Connel-Bronin, *Phys. Stat. Sol.* **38**, 1489, (1996).
33. G.F. Koster, J.C. Slater, *Phys. Rev.*, **95**, 1167,(1954);
34. G.F. Koster, J.C. Slater, *Phys. Rev.*, **96**, 1208,(1954);
35. J.H. Crawford, L.M. Slifkin (Eds.), Point Defects in Solids, Plenum, New York, (1972);
36. W. Hayes, A.A. Stoenham, Defects and Defect Processes in Non-Metallic Solids, Wiley, New York, (1985).
37. E. Kotomin, A. Popov, *Nucl. Instrum. Methods B* **141**, 1, (1998) and references therein.
38. R. Hilsch, R.W. Pohl, *Z. Phys.* **57**, 145, (1929); R. Hilsch, R.W. Pohl, *Z. Phys.*, **59** , 812, (1930).
39. A.S. Shalabi, A.M. El-Mahdy, *Phys. Lett.*, A **281**, 176, (2001); A.S. Shalabi, Kh.M. Eid, M.A. Kamel, Z.M. Fathi, *Int. J. Modern Phys. C* **11**, 1491, (2001).
40. A.S. Shalabi, A.M. El-Mahdy, M.A. Kamel, H.Y. Ammar, *Phys. B* **304**, 444, (2001).